ISSN 1070-3284, Russian Journal of Coordination Chemistry, 2022, Vol. 48, No. 9, pp. 592–599. © Pleiades Publishing, Ltd., 2022.

A New Supramolecular Hybrid Based on Keggin Polyoxotungstates and Dinuclear Cl-Bridged Cu(II) Complex: Synthesis, Characterization, and Properties

Y. B. Liu[a], *, J. J. Zheng[a], G. Tian[b], H. Wang[a], S. G. Alating[a], and J. S. Nie[a]

[a] *Department of Materials Science and Engineering, Jilin Jianzhu University, Changchun, 130118 P.R. China*

[b] *College of Chemistry and State Key Laboratory of Inorganic Synthesis and Preparative Chemistry, Jilin University, Changchun, 130023 P.R. China*

**e-mail: liuyab@163.com*

Received December 15, 2021; revised January 29, 2022; accepted January 31, 2022

Abstract—A new compound, $[Cu_2^{II}Cl(2,2'\text{-Bipy})_4]\{[Cu^{II}(2,2'\text{-Bipy})_2][BW_{12}^{VI}O_{40}]\}\cdot 2H_2O$ (**I**) (2,2'-Bipy = 2,2'-bipyridine), has been hydrothermally synthesized and characterized by elemental analysis, infrared (IR) spectroscopy, X-ray photoelectron spectroscopy (XPS), thermal gravimetric (TG) analysis, power X-ray diffraction (PXRD) and X-ray single-crystal diffraction analysis (CCDC no. 1936106). Compound **I** consists of a Keggin polyoxotungstate mono-supported Cu^{II}-2,2'-Bipy complex, a dinuclear Cl-bridged Cu(II) complex and two water molecules. The $[Cu_2^{II}Cl(2,2'\text{-Bipy})_4]^{3+}$ unit is a counter ion which is anchored to the polyanion via non-covalent intermolecular interaction. In addition, the fluorescence and both the catalytic performance for the epoxidation styrene and the photocatalytic property for degradation of Rhodamine B (RhB), Methylene blue (MB) and RhB + MB aqueous solutions under UV irradiation of compound **I** have been investigated and shown good properties.

Keywords: hydrothermal synthesis, polyoxotungstates, crystal structure, fluorescence, catalysis

DOI: 10.1134/S1070328422090020

INTRODUCTION

The polyoxometalates (POMs) represent a distinctive class of inorganic metal-oxygen clusters which are generally formed by groups VB, VIB transition metal (e.g., V^{5+}, Nb^{5+}, Mo^{6+} and W^{6+}) possessing unique topological and electronic diversities, and have extensive applications in the fields of photocatalysis, sensing materials, medicine, and nanotechnology, and so on [1–4]. Since the first Keggin type POM was reported by Keggin in 1933, the quantity of hybrids with POMs increased at an explosive rate supported by the technical amelioration of characterization methods and structural analysis, for example infrared spectroscopies, Raman spectroscopies, mass spectroscopies, nuclear magnetic resonance, and X-ray diffraction. Recently years, a new advance direction in POMs chemistry is built up hybrids with unprecedented structures constructed from the combination of POMs and transition metal complexes (TMCs) [5–18].

The study of hybrid compounds including halide ions, have been devoted by a several research groups, and a variety of those compounds were reported [19–32]. According to the role of halide ions in organic-inorganic hybrids, which could be split into four categories: (I) halide serve as patterns to construct novel hybrids and no covalent interactions with any atoms, the typical compounds such as $[H_2V_{18}^{IV}O_{42}(Cl)]^{11-}$ [19], $[Cu_{20}Cl(OH)_{24}(H_2O)_{12}(P_8W_{48}O_{184})]^{25-}$ [20], (II) halide ions act as terminal monodentate ligands linked by transition metal cations , and the compound such as $[Cu_3Cl(4,4'\text{-Bipy})_4][Cu(1,10\text{-Phen})_2Mo_8O_{26}]$ [21], (III) halide ions serve as bridge linked by POMs and TMCs, and the compounds include $\{[Cu(En)]_2[\alpha\text{-}PCuW_{11}O_{39}Cl]\}^{4-}$ and $\{[Cu(En)_2(H_2O)][Cu(En)_2]_2\text{-}[\alpha\text{-}PCuW_{11}O_{39}Cl]\}$ [22]; (IV) halide ions paly as multdentate ligand with transition metal cations and the examples including $(2,2'\text{-Bipy})Cu_3I_3$ [23], Cu_6I_6 [24], $[(CuX)_2(\mu_2\text{-pyrimidine-N,N'})]$ (X = Cl, Br, I) [25], $[Cu_{14}I_{14}(Dabco)_5(Py)]$ [26]. Compared with (I), (II) and (III) types, to the best of our cognition, the majority of reported the hybrid compounds containing halide ions is (IV) type, more interesting and important halide-bridged TMCs. However, the hybrids building up POMs and metal halides have been seldom reported in recently years. For example, Niu reported the first hybrid-based POMs anion

$[SeW_{12}O_{40}]^{2-}$ with $[Cu_2(2,2'\text{-Py})_2Cl]^+$ Cl-bridged Cu(I) compound cation [27]. Fortunately, the Lindquist-type $[Cu(4,4'\text{-Bipy})_4Cl][Cu(1,10\text{-Bipy})_2Mo_8O_{26}]$ [28], Keggin type $\{[CuCl(Phen)_2]_2\}(PMo_{12}O_{40})\cdot H_2O$ [29], $[Cu(Phen)_2]_4[Cu_5Cl_4(Phen)_4][PW_{12}O_{40}]_2\cdot 4H_2O$ [30], $[BW_{12}O_{40}]_2[CuCl(Phen)_4](H_2 4,4'\text{-Bipy})_4\cdot H_2O$ [31], and capped Keggin type $\{[PMo_{12}Sb_2O_{40}][(Cd(Phen)_2)_2Cl]\}$ [32] have been synthesized. Although POMs are widely used as green catalyst in H_2O_2-based oxidation reaction system, the functional materials building up POMs and halide-bridged TMCs applied in both photocatalysis and chemical catalysis are almost scarcely investigated [33–35].

Here in, we report hydrothermal synthesis and characterization of a new isolated hybrid compound: $[Cu^{II}_2(2,2'\text{-Bipy})_4Cl]\{[Cu^{II}(2,2'\text{-Bipy})_2][BW^{VI}_{12}O_{40}]\}\cdot 2H_2O$ (**I**) (2,2'-Bipy = 2,2'-Bipyridine). Compound **I** constructed from mono-supported Keggin POMs and dinuclear Cl-bridge Cu(II) cation with O···O, N–H···O and C–H···O hydrogen bonds interactions which displays a 3D supramolecular structure. Moreover, excellent fluorescence and catalytic properties toward the epoxidation of styrene and the photodegradation of Rhodamine B (RhB), Methylene blue (MB) and RhB + MB organic dyes of compound **I** were described and discussed.

EXPERIMENTAL

Material and methods. All chemical reagents were analytically pure and meet grade requirements without any further purification for use. The elemental analyses (C, H and N) were recorded on a PerkinElmer 2400 CHN elemental microanalyzer. Cu, B, W and Cl elemental analyses were performed on a Perkin-Elmer Optima 3300DV spectrophotometer. Infrared spectrum for solid sample was taken on a PerkinElmer spectrophotometer in the range of 4000–400 cm^{-1} by pressing KBr pellets. The powder X-ray diffraction (PXRD) pattern was determined on a XPertPro X-ray diffractometer using CuK_α radiation with a variable divergent slit and a solid-state detector. X-ray photoelectron spectrum (XPS) was collected on a Thermo ESCALAS 250 spectrometer by using a MgK_α (1253.6 eV) achromatic X-ray radiation source. Thermogravimetric (TG) analysis was collected by under a N_2 air flow with a heating rate of 10°C min^{-1} on Perkin-Elmer TGA-7000 thermal analyzer. Emission/excitation spectrum was carried out on a RF-540 fluorescence spectrophotometer. UV–Vis spectra were measured using a Shimadzu UV-3100 spectrophotometer at room atmosphere.

Synthesis of compound I. We have been obtained compound **I** by hydrothermal synthesis method [36]. $(NH_4)_6W_7O_{24}\cdot 6H_2O$ (1.01 g, 0.33 mmol), H_3BO_3 (0.092 g, 1.5 mmol), Sb_2O_3 (0.194 g, 0.66 mmol), $CuCl_2\cdot 2H_2O$ (0.113 g, 0.66 mmol), and 2,2'-Bipy (0.185 g, 1.2 mmol) were mixed in 18 mL distilled water, stirred for 60 min in air at room atmosphere. The pH value of the solution of mixture was adjusted to about 2 by using 4.0 M HCl. The stirred mixture was loaded into a 30 mL Teflon-lined stainless-steel autoclave and heated under autogenous pressure at 160°C for 72 h, then left to cool to normal temperature slowly at a rate of 4°C/h, washed and dried in air to obtain brown block crystals (the yield was 78.9% based on W). One brown block crystal suitable for X-ray diffraction was selected from the samples.

For $C_{60}H_{52}N_{12}O_{42}BClCu_3W_{12}$									
Anal. calcd., %	C, 17.77	H, 1.28	N, 4.14	Cl, 0.87	B, 0.27	Cu, 4.70	W, 54.40
Found, %	C, 17.63	H, 1.33	N, 4.14	Cl, 0.79	B, 0.35	Cu, 4.66	W, 54.43

X-ray crystallographic study. The crystal of compound **I** with size of 0.22 × 0.13 × 0.13 mm was reserved on a Bruker Smart CCD single crystal diffractometer sample holder at normal temperature to determine the crystal structure. Crystal data were collected in ψ-ω scanning mode using MoK_α rays (λ = 0.71073 Å) as the radiation source. We found no signs of crystal decay during single crystal data collection. Datarestoration using the SAINT procedure, direct method was used to solve the crystal structure by SHELXS-2018 program and the full matrix least squares on F^2 method was used to refine the crystal structure by the SHELXTL software package [37]. All non-hydrogen atoms were corrected for anisotropy except for crystalline water molecules. Hydrogen atoms were determined by the theoretical hydrogenation procedure. The crystal data and structure parameters are shown in Table 1, selective bond lengths and angles are listed in Table 2.

The supplementary cryatallographic data and more detailed information of compound **I** were stored in the Cambridge Crystallographic Data Centre (CIF file CCDC no. 1936106; http://www.ccdc.cam.ac.uk/data_request/cif).

RESULTS AND DISCUSSION

Single crystal structure analysis results show that the dissymmetric structural unit for compound **I** is made up of a classical Keggin polyanion connected to one copper complex $\{[Cu(2,2'\text{-Bipy})_2][BW_{12}O_{40}]\}^{3-}$, one copper chloride cation $[Cu_2(2,2'\text{-Bipy})_4Cl]^{3+}$ and two water of crystallization molecules. The well-known Keggin polyoxoanion can be described as a central $\{BO_4\}$ tetrahedron surrounded by a shell of $\{W_{12}O_{36}\}$ that are composed of four $\{W_3O_{13}\}$ tungsten triads, which is made up of three edge-sharing $\{WO_6\}$ distorted octahedra. The B–O bond lengths and OB(1)O angles are in the range of 1.506(8)–1.567(9) Å and 108.3(5)° to 111.3(5)° thereby showing that the $\{BO_4\}$ unit is an irregular tetrahedron. The W–O bond lengths fall into three types: O_t, O_b and O_c,

which is expressed terminal oxygen, bridging oxygen and central oxygen atoms, respectively. The W–O_t, W–O_b and W–O_c distances are 1.696(5)–1.724(5), 1.851(5)–1.967(5) and 2.306(4)–2.397(5) Å, respectively. The oxidation states of W atoms were calculated with reference to the bond valence parameters given by Brown [38]. The bond-valence sum (BVS) values for twelve independent W atoms are 5.72, 6.03, 6.09, 5.96, 5.96, 6.02, 6.02, 6.05, 5.98, 6.02, 6.12 and 6.06, respectively. The results show that the average value of twelve W atoms is 6.005, which show the formula is $[BW_{12}^{VI}O_{40}]^{5-}$.

Except for the $[BW_{12}^{VI}O_{40}]^{5-}$ polyoxoanion, there are two different crystallographic independent copper units. Transition metal coordination fragments $[Cu^{II}(2,2'\text{-Bipy})_2]^{2+}$ and metal halide fragments $[Cu_2^{II}(2,2'\text{-Bipy})_4Cl]^{3+}$ showing two kinds of different coordination types in **I**. The $[Cu^{II}(2,2'\text{-Bipy})_2]^{2+}$ fragment shows a square pyramidal coordination configuration with copper centers (Cu(1)) coordinated by four N atoms from two 2,2'-Bipy molecules, the Cu(1)–N bond lengths are changed from 1.970(6) to 2.058(6) Å, respectively. As illustrated in Fig. 1, one TMC cation $[Cu(1)(2,2'\text{-Bipy})_2]^{2+}$ is connected with one bridge oxygen atom (O(32)) from the Keggin polyanion $[BW_{12}^{VI}O_{40}]^{5-}$ skeleton with the Cu(1)–O(32) bond distance of 2.191(5) Å, forming one mon-supported $\{[Cu(2,2'\text{-Bipy})_2][BW_{12}O_{40}]\}^{3-}$ cluster anion. As shown in Fig. 2, the transition metal halide fragment is made up of two copper cations, one chloride anion and four 2,2'-Bipy ligands. The Cu(2) and Cu(3) ions have a semblable coordination environment which can be represented as distorted trigonal bipyramid. Cu(2) and Cu(3) are situated at a crystallographic center, coordinated by two 2,2'-Bipy groups with the bond distances of 1.977(7)–2.009(7) Å for Cu(2)–N and 1.982(7)–2.061(7) Å for Cu(3)–N, respectively. The chloride anion serves as a bridge connecting the two $[Cu(2,2'\text{-Bipy})_2]^{2+}$ transition metal complexes into a dinuclear Cl-bridged copper cation with the bond distances of 2.672(3) and 2.409(3) Å for Cu(2)–Cl(1) and Cu(3)–Cl(1), and the angle of 147.8(1)° for Cu(2)Cl(1)Cu(3). And then, two trigonal bipyramids are connected by sharing the chloride anion from $[Cu_2^{II}(2,2'\text{-Bipy})_4Cl]^{3+}$. The valence calculations show that the values for Cu(1), Cu(2) and Cu(3) atoms are 2.06, 2.03 and 2.05, respectively. The results show that the average value of copper atoms is 2.05, which is accordance with the formula of compound **I**.

It is also striking to note that many kinds of hydrogen bonds play an important role in stabilizing the crystal structure of compound **I**. The neighboring $\{[Cu(2,2'\text{-Bipy})_2][BW_{12}O_{40}]\}^{3-}$ cluster anions are linked to constitute a 1D supramolecular chains along *a* axis through O(11)···O(9) ($^{2\#}$ 1 + *x*, *y*, *z*) interactions between hydrogen bonds with the distances of 2.930(1) Å, as shown in the Fig. 3. The most particular form of **I** is that the O(*w*1) is further hydrogen-bonded to both O(1)2 from 1D supramolecular chains and O(6) from adjacent supramolecular chains with O(6)···O(*w*1) ($^{1\#}$ 2 − *x*, 1 − *y*, −*z*) and O(*w*1)···O(12) interactions between hydrogen bonds with distance of 2.956(1) and 2.908(1) Å along *b* axis. Thus, O(*w*1) acts as bridges interconnecting two adjacent chains into an interesting 1D supramolecular double chain.

Except for O···O and O–H···O hydrogen bonds, there are C–H···O and N–H···O hydrogen bonds between oxygens of $\{[Cu(2,2'\text{-Bipy})_2][BW_{12}O_{40}]\}^{3-}$ cluster and carbon or nitrogen atoms of copper halide cation $[Cu^{II}(2,2'\text{-Bipy})_2]^{2+}$ with the C···O and N···O distance of 3.028(1)–3.248(1) and 2.877(1)–3.317(1) Å. These O···O, O–H···O, C–H···O and N–H···O synergistic interactions increased the stability of **I**, and connected $\{[Cu(2,2'\text{-Bipy})_2][BW_{12}O_{40}]\}^{3-}$, metal halide cation $[Cu_2^{II}(2,2'\text{-Bipy})_4Cl]^{3+}$ and water molecules into a 3D supramolecular network (Fig. S1). This strong hydrogen bonding interactions of compound **I** are listed in Table 3.

Table 1. Crystallographic data and refinement details of the complexes **I**

Parameter	Value
Empirical formula	$C_{60}H_{52}BN_{12}O_{42}ClCu_3W_{12}$
Formula weight	4056.21
Crystal system	Triclinic
Space group	$P\bar{1}$
a, Å	13.1067(3)
b, Å	14.7311(3)
c, Å	22.1761(5)
α, deg	85.793(2)
β, deg	78.665(2)
γ, deg	83.981(2)
V, Å ^{3}	4168.90(16)
Z	2
ρ_{calcd}, g/cm^3	3.231
μ, mm^{-1}	17.355
θ Range, deg	2.890–25.049
Reflection collected	37762
Unique reflection (R_{int})	14747 (0.0350)
Goodness-of-fit on F^2	1.077
R indices ($I > 2\sigma(I)$)	R_1[a] = 0.0305, wR_2[b] = 0.0574
R (all date)	R_1 = 0.0409, wR_2 = 0.0617
$\Delta\rho_{max}/\Delta\rho_{min}$, e Å^{-3}	1.693/−1.300

[a] $R_1 = \Sigma\|F_o| - |F_e\|/\Sigma|F_o|$; [b] $wR = \{[\Sigma w(F_o^2 - F_e^2)^2]/[\Sigma w(F_o^2)^2]\}^{1/2}$.

Table 2. Selected bond lengths (Å) and bond angles (deg) for compound **I**

Bond	*d*, Å	Bond	*d*, Å
W(1)–O(13)	1.724(5)	W(2)–O(24)	1.708(5)
W(1)–O(40)	1.869(5)	W(2)–O(14)	1.884(5)
W(1)–O(20)	1.898(5)	W(2)–O(34)	1.901(5)
W(1)–O(38)	1.940(5)	W(2)–O(38)	1.907(5)
W(1)–O(32)	1.967(5)	W(2)–O(35)	1.926(5)
W(1)–O(1)	2.306(4)	W(2)–O(1)	2.375(4)
W(3)–O(7)	1.696(5)	W(4)–O(23)	1.885(5)
W(3)–O(26)	1.889(5)	W(4)–O(22)	1.942(5)
W(3)–O(3)	2.323(4)	W(4)–O(3)	2.397(5)
W(5)–O(8)	1.706(6)	W(6)–O(36)	1.866(5)
W(5)–O(19)	1.912(5)	W(6)–O(2)	2.359(5)
W(7)–O(10)	1.708(5)	W(8)–O(39)	1.878(5)
W(7)–O(39)	1.912(5)	W(8)–O(17)	1.934(5)
W(9)–O(11)	1.714(5)	W(10)–O(19)	1.884(5)
W(9)–O(26)	1.940(5)	W(10)–O(25)	1.927(5)
W(11)–O(30)	1.862(5)	W(12)–O(20)	1.903(6)
Cu(1)–N(3)	1.967(6)	Cu(2)–N(10)	1.976(7)
Cu(1)–N(1)	1.970(6)	Cu(2)–N(12)	1.998(8)
Cu(1)–N(4)	2.058(6)	Cu(2)–Cl(1)	2.672(3)
Cu(3)–N(8)	1.982(6)	B(1)–O(2)	1.506(7)
Cu(3)–Cl(1)	2.409(3)	B(1)–O(1)	1.567(9)
N(1)–C(5)	1.334(9)	N(2)–C(6)	1.367(9)
N(4)–C(20)	1.342(10)	N(9)–C(45)	1.336(11)
Angle	ω, deg	Angle	ω, deg
O(13)W(1)O(20)	101.2(2)	O(24)W(2)O(34)	100.6(2)
O(26)W(3)O(34)	91.8(2)	O(33)W(4)O(28)	159.0(2)
N(3)Cu(1)N(1)	177.3(3)	N(10)Cu(2)N(12)	165.0(3)
N(10)Cu(2)Cl(1)	82.1(2)	O(2)B(1)O(4)	111.3(5)
N(1)C(5)C(4)	122.2(8)	C(8)C(9)C(10)	118.7(9)

Table 3. Hydrogen bonds parameters (Å) for compound **I***

D–H...A	Distances, Å	D–H...A	Distances, Å
O(6)···O(*w*1)$^{\#1}$	2.956(1)	O(11)···O(9)$^{\#2}$	2.930(1)
N(4)–H···O(10)	2.877(1)	N(9)–H···O(25)	3.317(1)
N(10)–H...O(18)	2.884(1)	N(11)–H···O(25)	2.994(1)
C(22)–H···O(11)$^{\#1}$	3.173(1)	C(27)–H···O(18)$^{\#3}$	3.248(1)
C(29)–H···O(8)$^{\#3}$	3.028(1)	O(*w*1)···O(12)	2.908(1)
O(*w*2)···O(9)	2.930(1)	O(*w*3)···O(10)$^{\#4}$	2.915(1)

* Symmetric components for **I**: $^{\#1}$ $2-x, 1-y, -z$; $^{\#2}$ $1+x, y, z$; $^{\#3}$ $1-x, -y, -z$; $^{\#4}$ $-1+x, y, z$.

By reviewing the information, we found one analogue compound $[Cu_2(2,2'\text{-Bipy})_4Cl][Cu(2,2'\text{-Bipy})_2SeW_{12}O_{40}]\cdot 2H_2O$ has been already published in Niu's paper in 2006 [27]. However, there exit signification differences between compound **I** and analogue one. Firstly, the Keggin-type cluster in the Niu's com-

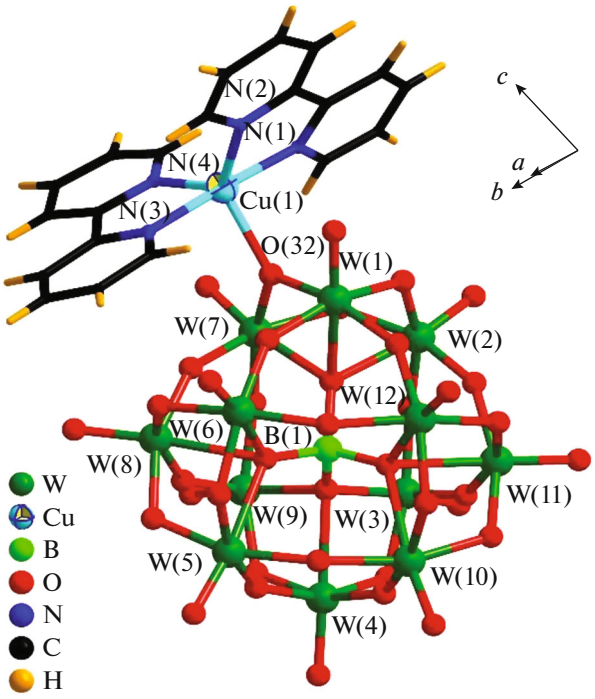

Fig. 1. Ball-stick representation of the Keggin polyoxoanion supported one $[Cu(2,2'\text{-Bipy})_2]^{2+}$ transition complex of **I**.

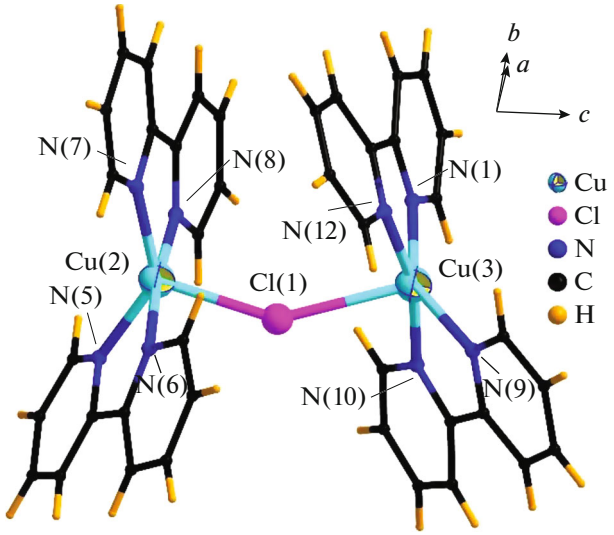

Fig. 2. The ball-stick and wire representation of the $[Cu_2(2,2'\text{-Bipy})_4Cl]^{3+}$ in compound **I**.

pound is not $[BW_{12}O_{40}]^{5-}$, but $[SeW_{12}O_{40}]^{2-}$. Secondly, though compound **I** contains many pyridine rings, however, the shortest distance between two pyridine rings facing each other is 4.527(1) Å. No strong π···π interactions exist in **I**. However, the π···π interactions are an important factor in the formation of the packing of structure in the Niu's compound. The last and most important, both the Niu's compound and the other group of hybrids built up POMs and copper halide units, almost all copper ions of metal halides are in the +1 valence, but the copper ions in compound **I** have a +2 valence. As far as we know, only one reported of Cu^{2+} based copper halide previously [29].

Figure S2 displays the FT-IR spectrum of compound **I**. The characteristic strong bands of $[BW_{12}O_{40}]^{5-}$ unit located at 953, 902, 802 and 769 cm^{-1} are ascribed to ν(B–O), (W–O_t), ν(W–O_b–W) and ν(W–O_c) stretching vibrations, respectively [39, 40]. A series of peaks in the regions of 1107–1664 cm^{-1} can be ascribed to vibrations of 2,2'-Bipy ligand. The broadband absorption peak nearly 3408 cm^{-1} belong to the vibration of the lattice water molecules of compound **I**.

XPS spectra of tungsten and copper atoms of compound **I** are displayed in Fig. S3. Two strong absorption peaks at 35.95 and 38.16 eV can be ascribed to the electron binding energies of W^{6+} $4f_{5/2}$ and W^{6+} $4f_{7/2}$, respectively (Fig. S3a); Shoulder peaks at 934.1 and 954.2 eV and satellite peak 942.6 eV ascribed to the electron binding energies of $Cu^{2+}2p_{3/2}$ and $Cu^{2+}2p_{1/2}$, respectively (Fig. S3b), we ascribed these peaks to the sites of W^{6+} and Cu^{2+} in compound **I** [41]. The XPS estimations of valences are consistent with the valence bond calculations for the W and Cu atom.

The experimental and simulated PXRD patterns of compound **I** are agreement with slight differences in the intensity of the peaks, indicating that **I** is the phase purity, as shown in Fig. 4. The differences in reflection intensities may be attributed to preferred orientations due to the crystalline powder samples of compound **I**.

The thermogravimetric (TG) analyses curves for compound **I** is presented in Fig. S4, which can be divided into three phases within 20–800°C. The first stage weight loss of 0.99% from 30 to178°C is consistent with the evaporation of two water molecules (calcd. 0.89%). The second stage weight loss of 16.33% in the range of 202–380°C is caused by the release of four 2,2'-Bipy ligands and a chloride ion (calcd. 16.27%). The third stage weight loss of 7.52% occurs between 383 and 625°C attributing to two 2,2'-Bipy molecules (calcd. 7.7%).

With DMSO solutions of 2,2'-Bipy and compound **I** to test the fluorescence performance was studied, and the curves of fluorescent spectra of 2,2'-Bipy and compound **I** at normal temperature are shown in Fig. 5. It can be seen as 2,2'-Bipy exhibits an emission peak at 415.1 nm upon excitation at 360 nm (Fig. 5a), and compound **I** displays an emission peak at 422.5 nm upon excitation at 364 nm (Fig. 5b). Because of similar emission bands is observed for a pure 2,2'-Bipy ligand that the photoluminescence mechanism of compound **I** can be assigned to intraligand transition.

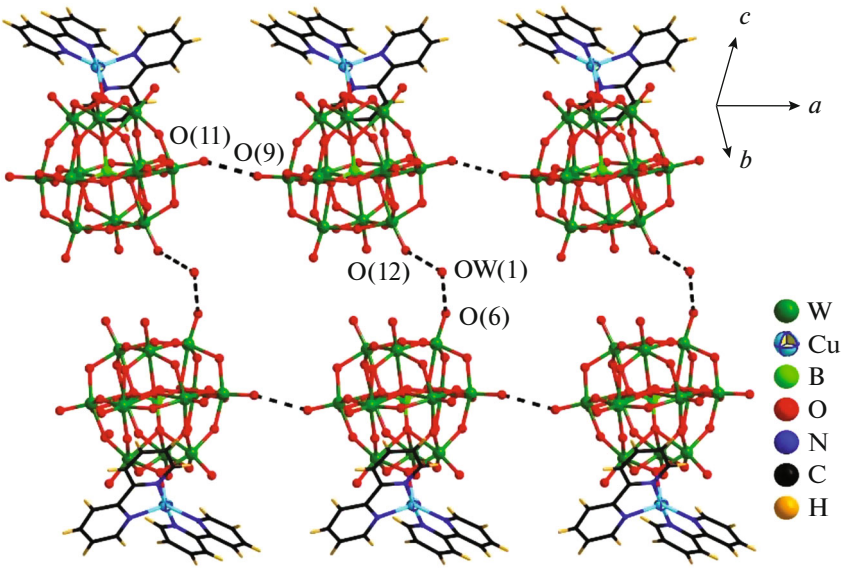

Fig. 3. View of 1D supramolecular double chains structure with hydrogen bonding interactions of **I**.

The catalytic performance of compound **I** was verified by the epoxidation of styrene-to-styrene oxide using aqueous tertbutyl hydrogen peroxide (TBHP) as a strong oxidant and compound **I** as catalyst in a batch reactor. Ground compound **I** (2 mg, 0.49 μmol), 0.11 mL styrene (1 mmol) and 2.5 mL acetonitrile were put in a 10 mL double-necked flask with a stirring device for reflux condensation. The epoxidation of styrene was started by filling the flask with 2 mmol TBHP when the oil bath was warmed to 80°C. The reaction will be lasted for 8 h, and the final composition of the organics in the reaction system was quantified using a GC-8A gas chromatograph (Shimadzu, GC-8A) equipped with an HP-5 capillary column and a hydrogen flame detector. The catalytic activity of the catalyst was also judged on the basis of the conversion of styrene and the selectivity of the products. Comparative experiments without the presence of catalyst showed no further reaction occurred after 8 h. Table 4 listed the reaction result of oxidation of styrene over the catalyst of compound **I** and shown an activity with 78.85% conversion and 57.80% selectivity to styrene oxide after 8 h. This information fully indication that compound **I** is excellent catalyst for the styrene epoxidation.

Typical industrial of organic dyes RhB and MB were chosen as dye contaminant to study the photocatalytic activity of compound **I** to evaluate its ability to purify industrial wastewater. The operating steps were as follows: (a) 5.0 mg of samples of compound **I** ground in an agate mortar for about 10 min was

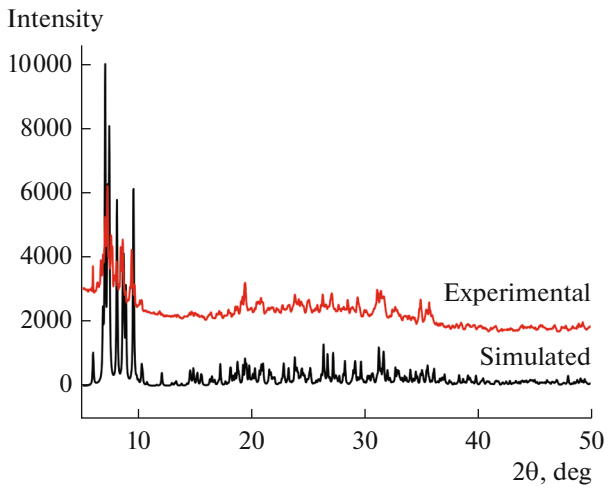

Fig. 4. The PXRD patterns of compound **I**.

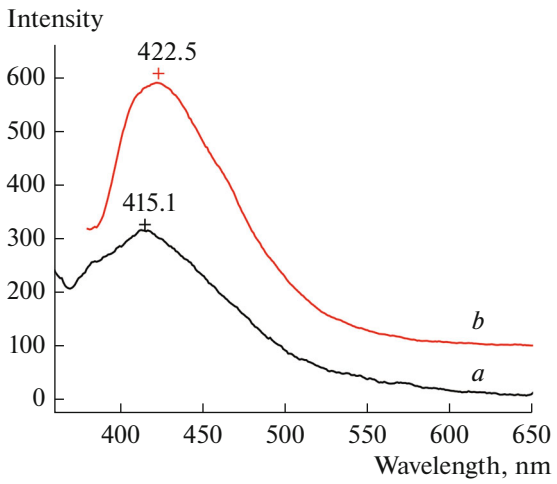

Fig. 5. Fluorescent spectra of DMSO solutions of 2,2'-Bipy (*a*) and compound **I** (*b*).

Table 4. Catalytic activity and product distribution of compound **I***

Catalyst	Styrene conversion, %	Product selectivity, %		
		So	Bza	others
No catalyst	0	0	0	0
Compound **I**	78.85	57.80	25.36	16.84

* So = styrene oxide; Bza = benzaldehyde; others = including benzoic acid and phenylacetaldehyde.

equally dispersed in 200 mL aqueous solutions (1.0×10^{-5} mol L^{-1}) of RhB, MB and RhB + MB system, respectively. (b) The suspension was stirred magnetically about 20 min in the dark, and 4 mL of the suspension was separated by centrifugation at 5000 rpm. The liquid supernatant was analyzed by UV–Vis spectroscopy and the data were recorded. (c) The reaction system was irradiated with a 400 W Xe lamp setting the liquid surface to lamp at 5 cm and centrifuged at 10000 rpm. Sample of 4 mL volume were removed every 20 min for analysis using UV–Vis spectroscopy. In the presence of compound **I** as a photocatalyst, the UV–Vis absorption spectra of photodegradations of the RhB, MB and RhB + MB solution with time were shown in Fig. 6, and changes in the conversion of the RhB, MB and RhB + MB solution (c_t/c_o) versus reaction time are plotted in Fig. S5. After 120 min reaction, the degradation rate reached 51% for the solution with only one RhB (Fig. 6a and Fig. S5a) and 99% for the solution with only one MB (Fig. 6b and Fig. S5b). The solution containing two mixed dyes (RhB + MB) reached 80% degradation for RhB and 99% degradation for MB at 100 min (Fig. 6c). It is worth noting that compound **I** shows excellent performance for the degradation of RhB in RhB + MB solution higher than that in pure RhB solution.

In this work, a new 3D supramolecular hybrid based on dodeca-tungstoselecnate and Cu^{II}-2,2'-Bipy complexes have been synthesized and structurally characterized. Compound **I** is composed of Keggin POM supported by TMCs and dinuclear Cl-bridged Cu(II) coordination cation. The oxidation states of all the copper atoms are +2 in compound **I** have been verified by the charge balance, valence sum calculations and XPS, and this result reveals that compound **I** represents for the second example building up POMs and copper(II) halide cation $[Cu_2^{II}(2,2'\text{-Bipy})_4Cl]$. Also, compound **I** shows good catalytic activities for the styrene epoxidation to styrene oxide with aqueous TBHP and the photocatalytic degradation-adsorption of RhB and MB under ultraviolet light irradiation. We will continue searching for novel hybrids containing the feature of both substructures of POMs and metal halides.

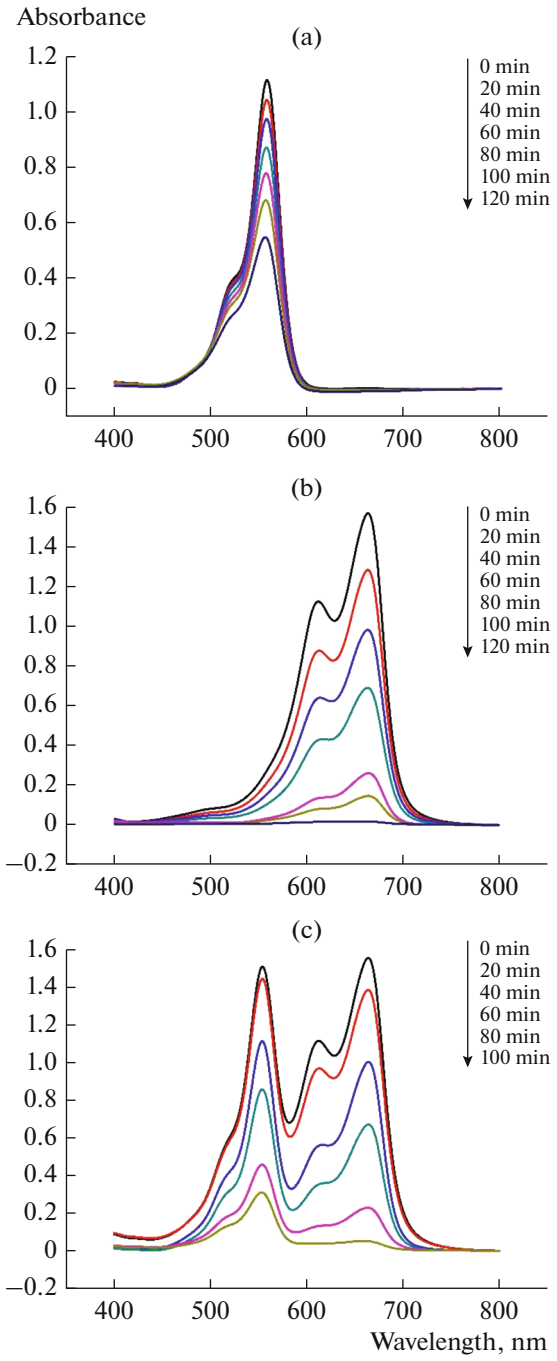

Fig. 6. UV–Vis absorption spectra of the RhB (a), the MB (b), and RhB + MB solution (c) under UV irradiation in the presence of compound **I**.

FUNDING

This work was supported by the National Natural Science Foundation of China (no. 51801070), Natural Foundation of Jilin Province (no. 20160101310JC), the 12nd 5-year and 13nd 5-year Science & Technology Research Program of the Department of Education of Jilin Province (nos. 2015258 and JJKH20180579KJ) and the science and technology development project of Jilin province, China (nos. 20190201286JC and 20210203098SF).

CONFLICT OF INTEREST

The authors declare that they have no conflicts of interest.

SUPPLEMENTARY INFORMATION

The online version contains supplementary material available at https://doi.org/10.1134/S1070328422090020.

REFERENCES

1. Pope, M.T., *Heteropoly and Isopoly Oxometalates*, Berlin: Springer, 1983.
2. Zhao, H.Y., Li, J.Y., Dong, D.P., et al., *J. Mol. Struct.*, 2021, vol. 1239, p. 130387.
3. Fan, X., Wang, J., Wu, K., et al., *Angew. Chem. Int. Ed.*, 2019, vol. 58, p. 1320.
4. Pope, M.T. and Muller, A., *Polyoxometalates: From Platonic Solids to Antiretroviral Activity*, Dordrecht: Kluwer Academic, 1994.
5. Pope, M.T. and Yamase, T., *Polyoxometalate Chemistry for Nano-Composite Design*, Dordrecht: Kluwer Academic, 2002.
6. Zheng, S.T., Zhang, J., Li, X.X., et al., *J. Am. Chem. Soc.*, 2010, vol. 132, p. 15102.
7. Bagtache, R., Meziani, D., Abdmeziem, K., et al., *J. Mol. Struct.*, 2021, vol. 1227, p. 129718.
8. Wang, S.S. and Yang, G.Y., *Chem. Rev.*, 2015, vol. 115, p. 4893.
9. Wang, L., Yang, W., Yi, F.Y., et al., *Chem. Commun.*, 2013, vol. 49, p. 7911.
10. Ying, J., Sun, C., Jin, L., et al., *CrystEngComm*, 2021, vol. 23, p. 5385.
11. Nie, J.S., Jiang, H.K., Pei, T.H., et al., *J. Changchun Univ. Sci. Technol.*, 2021, vol. 44, p. 97.
12. Zhu, Z.K., Lin, Y.Y., and Lin, L.D., *Inorg. Chem.*, 2020, vol. 59, p. 11925.
13. Zhang, B., Ying, J., Zhang, X., et al., *New J. Chem.*, 2020, vol. 44, p. 18074.
14. Zhang, X., Zhang, Y., Ying, J., et al., *J. Solid State Chem.*, 2021, vol. 295, p. 121888.
15. Liu, Y.B., Duan, W.J., Cui, X.B., et al., *Chem. J. Chinese Universities*, 2015, vol. 36, p. 34.
16. Sha, J.Q., Yang, X.Y., Zhu, P.P., et al., *RSC. Adv.*, 2016, vol. 6, p. 108328.
17. Lu, B., Li, S., Pan, J., et al., *Inorg. Chem.*, 2020, vol. 59, p. 1702.
18. Song, J., Wang, J., and Zhou, R., *Chem. Res. Chin. Univ.*, 2017, vol. 33, p. 333.
19. Müller, A., Sessoli, R., Krickemeyer, E., et al., *Inorg. Chem.*, 1997, vol. 36, p. 5239.
20. Liu, G., Liu, T., Mal, S.S., et al., *J. Am. Chem. Soc.*, 2006, vol. 128, p. 10103.
21. Hua, J., Qi, Y.F., Wang, E.B., et al., *Eur. J. Inorg. Chem.*, 2006, vol. 22, p. 4541.
22. Zhao, J.W., Zheng, S.T., and Yang, G.Y., *J. Solid State Chem.*, 2008, vol. 181, p. 2205.
23. Li, G.H., Shi, Z., Liu, X.M., et al., *Inorg. Chem.*, 2004, vol. 43, p. 6884.
24. Amoore, J.M., Hanton, L.R., and Spicer, L.R., *Dalton Trans.*, 2003, vol. 6, p. 1056.
25. Näther, C. and Jeß, I., *Eur. J. Inorg. Chem.*, 2004, vol. 14, p. 2868.
26. Hou, Q., Yu, J.H., Xu, J.N., et al., *CrystEngComm*, 2009, vol. 11, p. 2452.
27. Wang, J., Ma, P., and Niu, J., *Inorg. Chem. Comm.*, 2006, vol. 9, p. 1049.
28. Zhang, Z., Liu, J., Li, Y., et al., *J. Solid State Chem.*, 2010, vol. 183, p. 228.
29. Lu, X.M., Shi, X.D., Bi, Y.G., et al., *Eur. J. Inorg. Chem.*, 2009, vol. 34, p. 5267.
30. Xiao, L.N., Wang, Y., Pan, C.L., et al., *CrystEngComm*, 2011, vol. 13, p. 4878.
31. Wang, L.M., Fan, Y., Wang, Y., et al., *J. Solid State Chem.*, 2012, vol. 191, p. 257.
32. Xiao, L.N., Peng, Y., Wang, Y., et al., *Eur. J. Inorg. Chem.*, 2011, vol. 12, p. 1997.
33. Xiao, L.N., Zhao, C.X., and Shi, X.M., *CrystEngComm*, 2018, vol. 20, p. 969.
34. Guo, Y.H., Cui, L.P., Lv, J.H., et al., *J. Solid State Chem.*, 2020, vol. 292, p. 121605.
35. Iyer, A.K., Roy, S., Haridasan, R., et al., *Dalton Trans.*, 2014, vol. 43, p. 2153.
36. Feng, S.H. and Xu, R.R., *Acc. Chem. Res.*, 2001, vol. 34, p. 239.
37. Sheldrick, G.M. *SHELX-97, Program for Crystal Structure Solution*, Göttingen: Univ. of Göttingen, 1997.
38. Brown, I.D., *Structure and Bonding in Crystals*, New York: Academic, 1981.
39. Rocchiccioli-Deltcheff, C., Fournier, M., Franck, R., and Thouvenot, R., *Inorg. Chem.*, 1983, vol. 22, p. 207.
40. Fletcher, H., Allen, C.C., Burnsa, R.C., et al., *Acta Crystallogr., Sect. C: Cryst. Struct. Commun.*, 2001, vol. 57, p. 505.
41. Platzman, I., Brener, R., Haick, H., et al., *J. Phys. Chem. C*, 2008, vol. 112, p. 1101.